Close-to-patient podels for gastric cancer: from patient-derived xenograft towards a novel gastric cancer mini-tumor model

Hakuno, S.K.; Zonne, J.; Janson, S.G.T.; Wielen, A. van der; Kuhlemaijer, E.B.; Steenbakkers, M.; ... ; Slingerland, M.

OncoTargets and Therapy

Dovepress
Taylor & Francis Group

Open Access Full Text Article

ORIGINAL RESEARCH

Close-to-Patient Models for Gastric Cancer: From Patient-Derived Xenograft Towards a Novel Gastric Cancer Mini-Tumor Model

Sarah K Hakuno[1,*], Joëlle Zonneveld[1,*], Stefanus GT Janson[1], Anthea Van der Wielen[1], Eleonore B Kuhlemaijer[1], Maud Steenbakkers[1], Leonie Plug[1], Eveline De Jonge-Muller[1], Eduard P De Winter[2], Margreet R De Vries[2], Tom Van Wezel[3], Stijn Crobach[3], Lukas JAC Hawinkels[1,*], Andrea Vallés-Martí[1,*], Marije Slingerland[4,*]

[1]Department of Gastroenterology and Hepatology, Leiden University Medical Center, Leiden, the Netherlands; [2]Department of Surgery, Leiden University Medical Center, Leiden, the Netherlands; [3]Department of Pathology, Leiden University Medical Center, Leiden, the Netherlands; [4]Department of Medical Oncology, Leiden University Medical Center, Leiden, the Netherlands

*These authors contributed equally to this work

Correspondence: Lukas JAC Hawinkels, Department of Gastroenterology and Hepatology, Leiden University Medical Center, Leiden, 2300, the Netherlands, Tel +31 71 526 6736, Email l.j.a.c.hawinkels@lumc.nl

Purpose: Gastric cancer (GC) is the fifth most lethal form of cancer. Because of its late diagnosis, high intratumor heterogeneity, and the presence of a dense stromal compartment, GC is less susceptible to systemic treatments compared to other tumor types. Many systemic therapies, developed to support curative and palliative treatment for GC and other cancers, did not reach the clinic, which might be due to the fact that preclinical data, obtained from simple cell-based models, does not translate to the complex GC tumor structure and the occurrence of drug resistance. Therefore, this study is aimed to establish fibroblast-rich, close-to-patient models for GC and evaluate their robustness by comparison with the primary GC tissue from the respective patients.

Material and Methods: Five different GC models were established: I) a subcutaneous and II) orthotopic patient-derived xenograft (PDX) model, III) an in vitro patient-derived organoid (PDO) model, which was IV) subcutaneously engrafted in vivo, and V) co-cultured with GC fibroblasts to form a novel multicellular fibroblast-rich GC model. Histology, immunohistochemistry, mutational status and tumor/stroma composition were compared between the parental tissues and the various models.

Results: Both PDX models reflected the histological structure of the parental tissue, consisting of distinct parenchymal and stromal compartments. Primary tumor mutations were maintained in the PDX, as well as markers of clinical interest, like HER2. Orthotopic GC-PDX models showed high growth rates, accompanied by significant stromal accumulation. GC-PDOs showed histological similarities with parental tissues, maintaining the various histological phenotypes. Engrafted subcutaneously in mice, these organoids generated stroma-rich tumors. To mimic these features in vitro, we established a multicellular model composed of GC-associated fibroblasts and GC organoids, aggregating into complex multicellular structures with high similarity to parental GC tumor tissues.

Conclusion: We generated five close-to-patient GC models, which can potentially facilitate preclinical evaluations of novel therapies.

Keywords: stomach, carcinoma, stroma, patient-derived organoid, patient-derived xenograft

Introduction

Gastric cancer (GC) is the fifth most prevalent and lethal cancer, with close to 1 million new cases and approximately 650,000 deaths worldwide in 2022, respectively.[1] The lethality of GC is due to many factors, including late diagnosis, the highly metastatic capacity of the tumors, and tumor heterogeneity, based on histology, genomics, and topography. These characteristics contribute greatly to the relatively poor 5-year survival of around 35%.[2] The cornerstone of curative therapy for GC is a multidisciplinary treatment based on resection and chemotherapy, with or without adjuvant therapy.[3]

https://doi.org/10.2147/OTT.S586407
Received: 18 December 2025
Accepted: 14 March 2026
Published: 25 March 2026

Unfortunately, the conventional approach offers very limited clinical benefit for advanced GC, with a median survival of less than one year.[4] Hence, additional therapies have been introduced for GC, like trastuzumab, ramucirumab, nivolumab and ipilimumab, which have improved clinical efficacy, but have not substantially improved the prognosis for GC patients.[5] Next to the late diagnosis of GC, the relatively high occurrence of multidrug resistance, combined with the presence of an abundant and dense stromal compartment, seems to make GC less susceptible to targeted treatment than other tumor types.[6] Next to tumor cells, GC tumors are composed of a large stromal compartment. A high amount of stroma is associated with unfavorable clinicopathological prognostic factors and decreased survival.[7] Furthermore, patients with a high amount of stroma in the nodal metastases, especially when combined with a stroma-high primary tumor, were observed to have an even worse survival.[8]

The tumor stroma or tumor microenvironment (TME) consists of various cell types, including inflammatory cells, nerves, and vascular endothelial cells, and is involved in the growth and expansion of neoplastic tissue. Cancer-associated fibroblasts (CAFs) are the most abundant cell type in the TME. GCs, particularly those of the undifferentiated subtype, exhibit a massive infiltration of CAFs.[9] CAFs mainly secrete extracellular matrix (ECM) proteins and a wide range of cytokines, affecting cancer cell mobility, inducing cancer stem cell-like properties, impairing chemotherapeutic responses and promoting immune evasion.[10–12] Next to affecting cancer progression at the primary site, CAFs promote disseminated cancer cell survival, prepare tumor niches and support colonization at distant sites. While CAF viability remains largely unaffected by systemic treatment, they can restrict drug access as a result of excessive ECM deposition, increasing interstitial pressure, promoting drug degradation, and chemotherapy evasion via adhesion-mediated drug resistance.[13–17] Therefore, the presence of CAFs in preclinical models is crucial to evaluate the potential of novel therapeutic agents to advance to the clinic. Hard-to-treat and stroma-rich cancers, like GC, might require extra attention for inclusion of the TME to optimize the full potential of novel (neo)adjuvant therapies. Like for any new therapy, exploration of the mechanisms of action and optimization of the intended effects must be elucidated in relevant preclinical settings. Although monolayer in vitro cell culture experiments, followed by subcutaneous cellular engrafting in immunodeficient mice, have shown their practical use for decades, the recent insights about the role of the TME demand more representative models. Multicellular modelling, like co-cultures of cancer cells with immune or stromal cells, organoid-on-a-chip models, patient-derived organoids (PDOs), orthotopic and humanized xenografts (PDXs), will become the standard of close-to-human, personalized, and preclinical research.[18–20]

In this study, we generated and evaluated a range of novel multicellular, organotypic GC models, by comparing them to their respective primary patient tumors. These multicellular models will potentially be crucial representative pre-clinical tools to optimally evaluate the effect of advanced combination therapy strategies on defined patient groups or single patients.

Patients, Materials and Methods

Patient Samples

Written informed consent for study participation was provided by all included gastric cancer patients. Human cancer tissue samples were obtained after gastric tumor resection surgery from the Leiden University Medical Center (LUMC, Leiden, the Netherlands) and used in an anonymized manner, adhering to the established guidelines of the Medical Ethical Committee of the LUMC, and conducted in accordance with the Declaration of Helsinki and the Code of Conduct for responsible use of Human Tissue and Medical Research as drawn up by the Federation of Dutch Medical Scientific Societies in 2011. The Code allows for the additional utilization of coded residual (historical) tissue and data derived from the diagnostic process for scientific purposes. Studies described in this work were approved by the Biobank Committee of the Medical Ethics Committee of the Leiden University Medical Center (RP24.004, B21.036, B20.035).

Patient-Derived Organoids

In order to generate PDOs from patient tumor tissue, tissues were washed three times with phosphate-buffered saline (PBS) (Fresenius Kabi, Netherlands), minced and digested by incubating with collagenase II (Gibco, Paisly, UK) for 2 hours at 37°C. After digestion, cells were passed through a 70 μm cell strainer and washed twice in Advanced

Dulbecco's Modified Eagle Medium (DMEM)/F12 medium (Gibco). Cells were resuspended in growth factor reduced Matrigel (Corning, New York, USA) and plated in 50 µL dome-shaped droplets per well. After the Matrigel solidified at 37°C, GC-PDO media was added to the wells. Optimized GC-PDO medium was prepared as described earlier.[21] Upon growth of the GC-PDOs, cells were passaged and expanded until passage 3 after which they were considered established cultures. PDOs were passaged once a week in a 1:2 ratio. Medium was removed from the PDO-containing Matrigel domes, the Matrigel was broken up with cold Advanced DMEM/F12 medium and the PDOs were separated from the Matrigel via centrifugation. The PDOs were dissociated mechanically in advanced DMEM/F12 medium with a syringe (1 mL BD Luer-Lok Tip, Becton, Dickinson and Company, Franklin Lakes, USA) and needle (30 g BD Microlance 3, Becton, Dickinson and Company). After centrifugation and separation of the dissociated PDOs, the cells were resuspended in Matrigel and plated in a 50 µL dome-shaped droplet per well (24-well flat bottom plate, Costar, Kennebunk, USA). PDOs were cultured in a humidified incubator at 37°C and 5% CO_2. Medium was replaced every 2–3 days.

Patient-Derived Fibroblasts

Patient-derived fibroblasts were isolated as described before.[20,22] In short, GC or adjacent normal gastric tissues were minced and digested using a mix of collagenase II (Gibco, Leiden, The Netherlands) and dispase II (Roche, Basel, Switzerland) in a 3:1 ratio for 2 hours at 37°C. Cells were cultured in DMEM/F12 containing 8% Fetal Calf Serum (FCS), 100 IU/mL penicillin and 100 µg/mL streptomycin (Thermo Fisher Scientific) in a humidified incubator at 37°C and 5% CO_2. After expansion, cells were tested for expression of fibroblast markers (collagen 1a1 and αSMA) and absence of epithelial (E-cadherin), endothelial (CD31) and immune (CD45) markers via qPCR (Table 1).

GC Mini-Tumor Models

Suspension co-cultures were established by dissociating PDOs and patient-derived fibroblasts as described above. PDOs and patient-derived fibroblasts were mixed at a ratio of 1:1.5 and 1.5:1 for mini-tumor 1 and 2, respectively, in co-culture-specific media containing 1% Matrigel. This media contained the same constituents as the GC-specific PDO medium, but without TGF-β inhibitor (A83-01) and with 10 µM ROCKi (Y-27632). Subsequently, a total of 10,000 cells per well were seeded in ultra-low attachment 96-well round-bottom plates (Corning). Plates were then centrifuged at 1500 rpm, at room temperature (RT) for 1 minute and incubated overnight at 37°C and 5% CO_2. After 24 h, medium was carefully removed from the wells. Co-cultures were then cultured in fibroblast medium mixed with 1% Matrigel until the end of the experiment. Medium was changed every 2–3 days.

Mice

All animal experiments were approved by the Dutch Central Committee on Animal Experimentation (permit numbers AVD116002017858 and 116002016549) and the Animal Welfare Body (IvD) of the LUMC Leiden and are in accordance with the Dutch Experiments on Animals Act and EU Directive 2010/63/EU. NSG mice (NOD.Cg-*Prkdc*^{scid} *Il2rg*^{tm1Wjl}/SzJ, male and female, in-house breeding) were used (8–16 weeks of age; 25–35 g) and housed in individually ventilated cages (n=4 mice per cage). Animals had *ad libitum* access to water and food pellets.

Table 1 Primers Used for Validation of Fibroblast Expression Markers

Target	Forward	Reverse
Col1a1	5' GATTCCCTGGACCTAAAGGTGC 3'	5' AGCCTCTCCATCTTTGCCAGCA 3'
αSMA	5' CCGGGAGAAAATGACTCAAA 3'	5' GAAGGAATAGCCACGCTCAG 3'
E-cadherin	5' GCCCCATCAGGCCTCCGTTT 3'	5' ACCTTGCCTTCTTTGTCTTTGTTGGA 3'
CD31	5' GCTGACCCTTCTGCTCTGTT 3'	5' TGAGAGGTGGTGCTGACATC 3'
CD45	5' AACAGTGGAGAAAGGACACA 3'	5' TGTGTCCAGAAAGGCAAAGC 3'
β-actin	5' GCACAGAGCCTCGCCTT 3'	5' GTTGTCGACGACGAGCG 3'

Subcutaneous GC-ODX Model

For the development of an organoid-derived xenograft (ODX), GC-PDOs were dissociated mechanically and separated from the Matrigel via centrifugation. PDOs were resuspended in cold advanced DMEM/F12 medium, further dissociated using a needle (25 g BD Microlance 3 needle, Becton, Dickinson and Company) and washed in medium. Suspensions of 50 organoids per 100 µL Matrigel were prepared for injection. Suspensions were injected subcutaneously in one or both flanks of NSG mice. Tumor growth and mice weight were monitored for 21 days.

Subcutaneous GC-PDX Engraftment and Expansion

For PDX engraftment, NSG mice of 8–16 weeks were subcutaneously injected 30 minutes before surgery with 3 µL/g Buprenorphine (Temgesic). Next, animals were anesthetized with a vaporized isoflurane gas system (0.06 L/min oxygen, 0.04 L/min air, 4% isoflurane for induction, and 2% for maintenance). After shaving, the flanks were cleaned with 70% ethanol. Gastric tumor pieces of 1×1 mm were kept in PBS on ice. Before implantation, pieces were washed in cold PBS and placed under the skin in a 2–3 mm incision. Once the incision was closed, mice were monitored daily during the first week, and weekly afterwards. If no tumor growth was observed after 12 months, the engraftment was considered unsuccessful. Tumor volume was calculated with the formula: short side^2 * long side. Once tumor volume reached a maximum of 1000 mm^3 (one flank) or 1500 mm^3 (two flanks combined), the tumor was removed and passaged until P3 in recipient mice.

Orthotopic GC-PDX Model

In order to develop an orthotopic GC model, tumor fragments were prepared from a previously established subcutaneous GC-PDX mouse. After euthanizing the mouse, the subcutaneous tumor was removed using sterile technique, kept in PBS on ice and immediately used for implantation of the orthotopic model. Mice received pre-operative analgesia via subcutaneous injection of 3 µL/g Buprenorphine (Temgesic) 30 minutes before the surgery. Mice were anesthetized as described above, and after shaving and cleaning with 70% alcohol, a midline abdominal incision of 1–2 cm was made. The abdominal peritoneal wall was opened, and the stomach was carefully exteriorized on a wet gauze using blunt forceps. The gastric serosa of the greater curvature was lightly damaged with a small needle. PDX fragments of 2×2 mm were implanted into the greater curvature of the stomach using a 6–0 suture. The stomach was repositioned in the abdominal cavity with a wet cotton swab, and the muscular layer and skin were closed with continuous and separate stitches, respectively, using 6–0 suture. Four to six hours after surgery, mice received a second injection of Buprenorphine. Wellness checks were performed daily during the first week, and three times per week thereafter.

Ultrasound Analysis

Ultrasound measurements were performed three weeks after surgery using the Vevo3100 imaging system (Fujifilm VisualSonics). Mice were anesthetized as described above and depilated. During ultrasound imaging, mice were placed under a heating lamp in the supine position, with continuous monitoring of heart rate, respiration, and body temperature. Images of the tumors were obtained in the sagittal plane (long axis) with the MX550D transducer at an axial resolution of 40 µm. Small-mouse (abdominal) mode was used with liver imaging presets to obtain images with a depth of 14 mm. Images were obtained using B-mode to quantify tumor location and volume and were analyzed using Vevo LAB 5.8.2 software. Additional Doppler ultrasound images were acquired in color mode to visualize angiogenesis in the tumors.

Histology and Immunohistochemical Analyses

Tissue was fixed, dehydrated, and processed to paraffin, as described previously.[23] 5 µm sections were stained with Hematoxylin (EMD Millipore Corporation, Amsterdam, the Netherlands) and 10 g/L Eosin (Merck, Darmstadt Germany) (H&E) or 10 g/L Alcian Blue (Merck, Darmstadt Germany). Immunohistochemically staining was performed using primary antibodies; mouse anti-αSMA (clone: 1A4/ASM-1, Progen, Heidelberg, Germany), mouse anti-Pan-Cytokeratin (pan-CK) (clone: PKC-26, Sigma-Aldrich, Zwijndrecht, the Netherlands), rabbit anti-Vimentin (clone: D21H3, Cell Signaling Technologies, Leiden, the Netherlands), rabbit anti-human Ki67 (SP6, Abcam, Cambridge, UK), rabbit anti-

Cleaved Caspase 3 (CC3) (clone: Asp175, Cell Signaling Technologies, Leiden, the Netherlands) and rabbit anti-Human Epidermal Growth Factor Receptor 2 (HER2) (DAKO, Carpinteria, USA). Sections were deparaffined, and endogenous peroxidase was blocked using 0.3% H_2O_2 in methanol, rehydrated and underwent antigen retrieval by boiling sections in 0.1 M sodium citrate (pH 6.0) buffer. Next, the sections were either washed in 1% BSA/PBS or blocked using TENG-T or 10% goat serum and washed (see Supplementary Table 1). Sections were incubated with primary antibodies overnight. The next day, the slides were washed and incubated with biotinylated secondary antibodies (DAKO, Carpinteria, USA, or Abcam, Cambridge, UK), washed and incubated with Vectastain complex (Vectorlabs, Peterborough, UK). The color was developed using 3,3′Diaminobenzidine (Abcam, Cambridge, UK). Nuclear staining was performed using Hematoxylin. Slides were dehydrated and mounted using Entellan™ (Merck, Darmstadt, Germany). Representative pictures were taken with an Olympus BX51TF microscope (Olympus Life Science Solutions, Zoeterwoude, the Netherlands).

Immunofluorescence

For immunofluorescence, sections were deparaffined, rehydrated and antigens were retrieved by boiling in sodium citrate as described above. Sections were incubated with the previously mentioned primary antibodies for mouse anti-Pan-CK and rabbit anti-Vimentin, washed and incubated with secondary antibodies, goat anti-rabbit Alexa Fluor 488 (Thermo Fisher Scientific, Landsmeer, the Netherlands) and goat anti-mouse Alexa Fluor 594 (Thermo Fisher Scientific, Landsmeer, the Netherlands). The sections were mounted using ProLong Gold Antifade mountant with DAPI (Invitrogen, Landsmeer, the Netherlands). Representative images were taken using the Leica DM6 microscope (Leica, Wetzlar, Germany).

DNA Next-Generation Sequencing

Mutation detection using DNA Next-Generation Sequencing (DNA NGS) was performed with a customized Cancer Hotspot Panel as described previously.[24]

In brief, AmpliSeq (ThermoFisher Scientific, Waltham, MA) NGS libraries were prepared following manufacturer's instructions. Barcoded libraries were pooled and loaded on S5 Chips using the Ion Chef (ThermoFisher Scientific), sequencing was performed on an Ion GeneStudio S5 Series sequencer (ThermoFisher Scientific). Unaligned sequenced reads were mapped against the human reference genome (GRCh37/hg19) using TMAP software and variants were called using Torrent Variant Caller (TVC) using default parameters for somatic variant calling.

Variant interpretation was performed with Genetic Assistant (Softgenetics).

Results

In this study, we established several close-to-patient models for GC to enhance the translational relevance of preclinical studies. Representative models can provide valuable information of the patient tumor characteristics and serve as a close-to-patient platform to facilitate the optimal evaluation of therapeutic targets that can potentially reach the clinical stage. Considering the significant stromal accumulation in GC tissue, we assessed the representativeness of stroma content in all in vitro and in vivo models by evaluating histology, mutational spectrum, and expression of the HER2 therapeutic target.

GC Patient-Derived Organoid Models (GC-PDO)

First, we aimed to establish an in vitro model system to study GC behavior. Surgically obtained human resection material was processed into single cell suspensions and seeded into Matrigel domes to establish PDO cultures (Figure 1A).

Histologically, GC-PDOs formed complex structures with varying phenotypes, from cystic sphere-shaped organoids with fluid-filled lumen (Figure 1B I and II) to more intermediate (Figure 1B III) and solid phenotypes (Figure 1B IV).

Immunohistochemistry-stained PDOs showed similar histological features compared to their parental tissues, with reflective Pan-CK and Alcian Blue staining for epithelial and mucus-producing cells, respectively (Figure 1C).

Furthermore, PDOs had high proliferation and low apoptotic rates, as shown via Ki67 and CC3 staining, comparative to their parental tissue (Figure 1D).

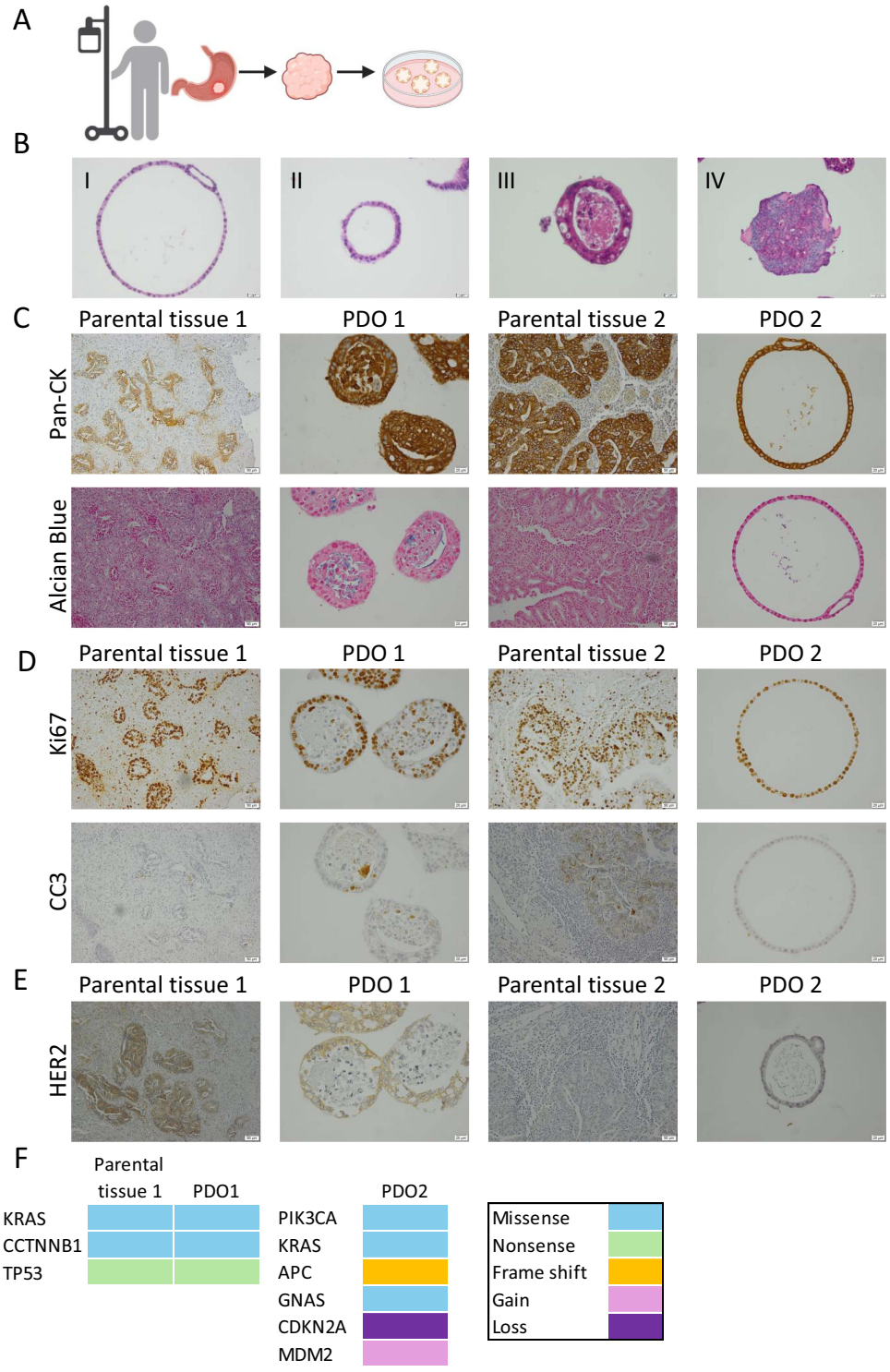

Figure 1 Establishment and evaluation of patient derived organoids (PDO). (**A**) GC-PDOs were generated from human GC material. (**B**) Different phenotypes of gastric PDO's: I and II cystic, III intermediate and IV solid. (**C–E**) Evaluation of the presence of biomarkers in cystic and solid PDO's in comparison with the original tissue from the patient. (**F**) Comparison of gene mutations in parental versus PDO tumor tissue. Scale bar for PDOs and parental tissues represent 20 µm and 50 µm, respectively. *Created in BioRender. Zonneveld, J (2026)* https://BioRender.com/0eu2ln3.
Abbreviations: PDO, patient-derived organoid; Pan-CK, pan-cytokeratin; CC3, cleaved-caspase 3; HER2, human epidermal growth factor receptor 2.

We evaluated the expression of HER2, a tumor marker and therapeutic target for the treatment of GC. HER2 expression status was maintained in the PDOs, where PDO1 remained HER2 positive and PDO2 HER2-negative (Figure 1E).

https://doi.org/10.2147/OTT.S586407

Hotspot mutation sequencing of the PDOs confirmed that all PDOs were cancerous and revealed a similar mutational spectrum to the parental tumors. For parental tissue 2, hotspot data was not available (n.a.) (Figure 1F).

Together, these data show that the generated and expanded GC-PDOs were reflective of parental GC tissues.

In vitro GC Mini-Tumor Model

Next, to be able to study tumor cell-CAF interaction in vitro, we established a GC mini-tumor model, as we have previously developed as well for pancreatic cancer.[20] CAFs were isolated from GC tissues and expanded. Fibroblasts had confirmed expression of fibroblast markers and did not express epithelial and immune cell markers (Supplementary Figure 1A). GC-PDOs were seeded with CAFs in a 1:1.5 (mini-tumor 1) and 1.5:1 (mini-tumor 2) ratio in suspension culture plates, and co-cultures were established. Samples were then followed over time and harvested, embedded and processed for immunofluorescence and immunohistochemistry (Figure 2A).

GC mini-tumors assembled into dense structures one day after seeding and continued to grow over the span of 7 days (Supplementary Figure 1B). Staining for the epithelial marker pan-CK and stromal marker vimentin showed complex multicellular structures, which differed per mini-tumor. Mini-tumor 1 consisted of a tumor cell-rich periphery with a dense fibroblast center and mini-tumor 2 showed islands of tumor cells surrounded by the dense fibroblast structures, which resembled the different parental tissues. These mini-tumors had similar αSMA levels and similar amounts of mucus-producing cells when compared to their parental tissue (Figure 2B). Immunofluorescence for pan-CK and vimentin showed fibroblast-dense centers surrounded by epithelial cells for mini-tumor 1 and a more mixed phenotype for mini-tumor 2, which further confirmed the results from immunohistochemistry (Supplementary Figure 1C). Ki67 and CC3 stainings showed high proliferation in the epithelial cells and overall low apoptotic rates, respectively (Figure 2C). HER2 expression status was maintained in both mini-tumor models (Figure 2D).

Both mini-tumors showed a unique phenotype with parental tumor characteristics mimicked in vitro. These results indicate that GC mini-tumors could be generated in a reproducible manner and resembled the parental tumor tissue they were derived from.

Subcutaneous GC-ODX Model

Given the lack of stromal cells in the PDO cultures and physiological relevance, we wondered if engraftment of the PDOs in NSG mice would result in stroma-rich or -poor tumors. GC-PDOs were expanded and injected subcutaneously into NSG mice (Figure 3A). Tumor growth was followed by caliper measurements, while mouse weight remained stable over the course of this experiment (Supplementary Figure 2A). PDO engraftment was successful in all evaluated mice (n=5). Tumors grew rapidly over the span of 21 days to reach a size of approximately 1000 and 1500 mm^3 (Figure 3B).

Hotspot mutation sequencing revealed that the engrafted organoids maintained the mutational spectrum of the original PDOs (Supplementary Figure 2B). Subcutaneously engrafted organoids resulted in stroma-rich GC tumors, with varying rates of stroma accumulation. Differentiation of tumor cells into mucus-producing cells was similar in the two ODX samples compared to parental tissue (Figure 3C). ODX tumors were highly proliferative, showed low apoptotic rates and contained vasculature, comparable to the parental tissue (Figure 3D). Low HER2 expression on the epithelial cells, as observed in the parental tissues, was maintained in the ODX tumors (Figure 3E).

These data show that subcutaneously injected organoids give rise to stroma-rich tumors and maintain histological characteristics of the parental tissue.

Subcutaneous GC-PDX Model

Similarly, we established a human GC patient-derived xenograft (GC-PDX) model via subcutaneous implantation of human GC material (scPDX) (Figure 4A). After implantation, tumors grew under the skin and were measurable by caliper after 6–27 weeks (Figure 4B).

Mouse weight remained stable throughout the experiment for all generations (Supplementary Figure 3A–E).

The first generation (G0) tumors were measurable by caliper after 27 weeks and reached the endpoint at 30 weeks. Tumors were harvested and subsequently engrafted in G1 recipient mice. Tumor engraftment of G1 mice was faster compared to G0 and tumors were measurable after 7 weeks, harvested after 8 weeks and engrafted in G2 mice, where

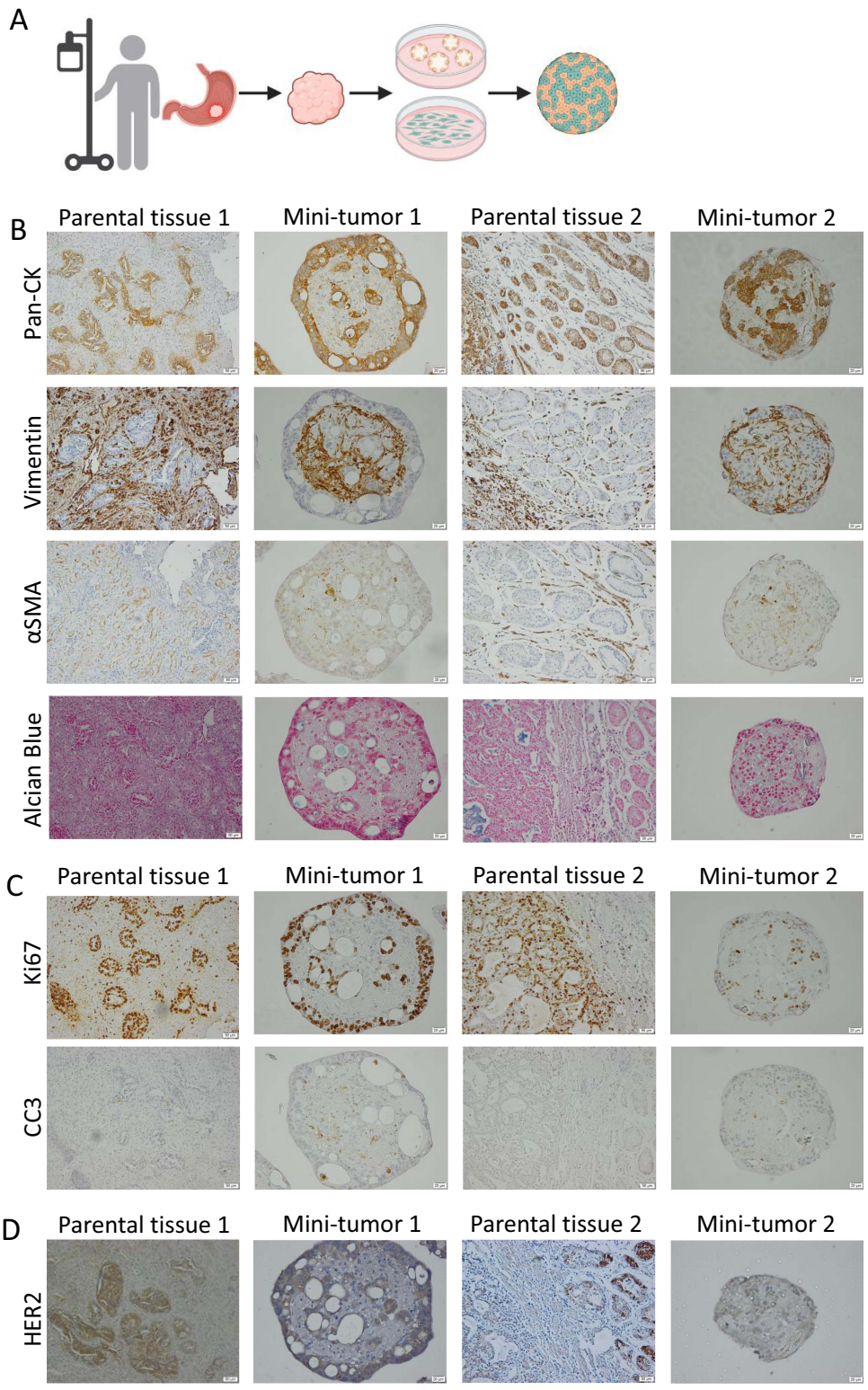

Figure 2 Establishment and evaluation of GC mini-tumors composed of PDOs and CAFs. (**A**) GC mini-tumors were generated with the use of human GC-PDOs and CAFs. (**B–D**) Histological stainings of the two mini-tumors and their corresponding parental tissue. Scale bar for minitumors and parental tissues represent 20 μm and 50 μm, respectively. *Created in BioRender. Zonneveld, J (2026)* https://BioRender.com/w79q93i.
Abbreviations: Pan-CK, pan-cytokeratin; CC3, cleaved-caspase 3; αSMA, alpha-smooth muscle actin.

https://doi.org/10.2147/OTT.S586407

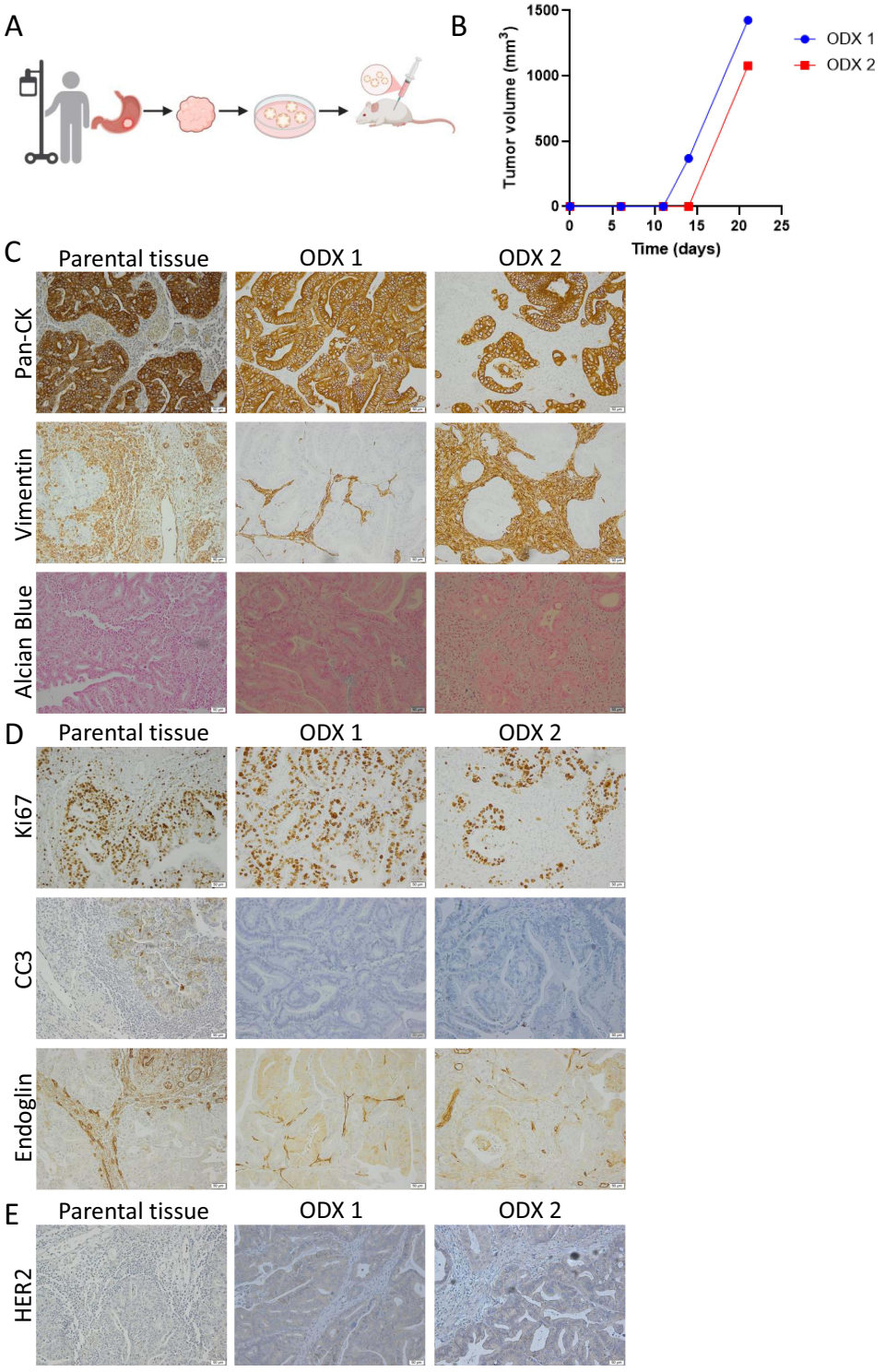

Figure 3 Subcutaneous injection of organoids leading to stroma-rich gastric cancers in two mice. (**A**) GC-PDOs were subcutaneously injected into NSG mice. (**B**) Tumor growth of subcutaneously injected GC-PDOs in mice. Data points represent growth of tumor in one flank in two different mice. Monitoring of mice weight after GC-PDO injection. (**C–E**) Histological stainings of two harvested tumors compared to the parental tissue. Scale bar represents 50 µm. *Created in BioRender. Zonneveld, J (2026)* https://BioRender.com/.favxy96.

Abbreviations: PDO, patient-derived organoid; Pan-CK, pan-cytokeratin.

https://doi.org/10.2147/OTT.S586407

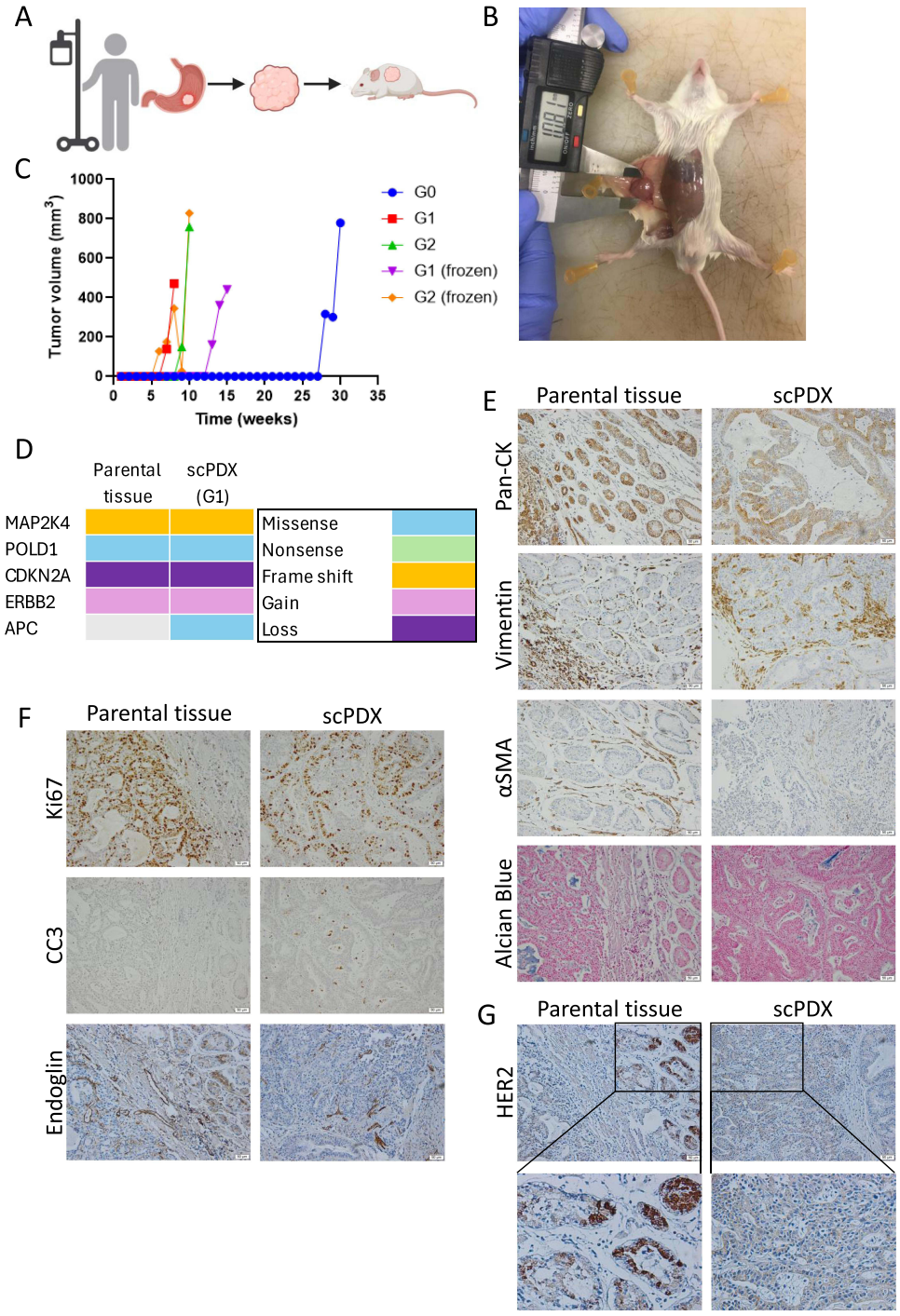

Figure 4 Establishment and evaluation of subcutaneous gastric cancer model (**A**) Patient-derived human gastric cancer tissue was subcutaneously xenografted in NSG mice. (**B**) Tumors grew rapidly under the skin. (**C**) Establishment and evaluation of tumor outgrowth was monitored for 30 weeks post transplantation for G0, G1, G2 and frozen G1 and G2. Data points represent one tumor. (**D**) Comparison of gene mutations in parental versus PDX tumor tissue. (**E** and **F**) (Immune)histochemical evaluation and comparison of parental and PDX tissue architecture. (**G**) Evaluation of the presence of characteristic tumor marker HER2 in parental versus PDX tissue. Scale bar represents 50 µm. *Created in BioRender. Zonneveld, J (2026)* https://BioRender.com/fl3ludj.

Abbreviations: PDX, patient-derived xenograft; Pan-CK, pan-cytokeratin; αSMA, alpha-smooth muscle actin; CC3, cleaved-caspase 3; HER2, human epidermal growth factor receptor 2.

tumors were measurable after 9 weeks. Additionally, G1 tumors were slow frozen and afterwards retransplanted in recipient mice. Tumors grew rapidly and were measurable by caliper after 13 weeks. The second passage of the frozen tissue engrafted even faster in recipient mice and could be measured after 6 weeks. The implantation success rates for G0, G1, G2, frozen G1 and frozen G2 were all 100%. Overall, tumor engraftment was quicker after PDX passages, by approximately 3-fold when comparing G1 and G2 to G0. Tumor engraftment was not affected by cryopreservation prior to implantation, demonstrating the utility of this model (Figure 4C).

Next, we analyzed the tumor mutational spectrum using DNA sequencing. Both the parental tissues and the grafted PDX samples showed a MAP2K4 frameshift mutation, a POLD1 missense mutation, loss of CDKN2A and gain of ERRB2, the gene coding for tumor marker HER2 (Figure 4D). In the PDX tumor tissue, a missense mutation in APC was detected, which did not appear in the parental tissue (Figure 4D).

Furthermore, we evaluated the histological features on the parental tissue and PDX (Figure 4E–G). G1 PDX was compared to parental tissue focused for epithelial cell marker pan-CK, stromal and mesenchymal cell markers vimentin, alpha smooth muscle actin (αSMA), a marker of pericytes and myofibroblastic cells, and Alcian Blue staining as indicator of cell differentiation. GC epithelial cells were similarly present on both source and model tissue sections, showing a comparable nodular growth. The same was true for the vimentin staining, which was similarly present in both tissues and surrounded the pan-CK-positive cells. With respect to αSMA, this staining was not homogeneously distributed in both tissues, but present at specific sites, probably depending on the differentiation state of the fibroblasts. Alcian Blue staining showed similar differentiation into mucus-producing cells both in the parental and PDX samples (Figure 4E). We analyzed Ki67, CC3 and endoglin, which showed similar proliferation, apoptosis and vascularization rates in GC tumors and the derived PDX (Figure 4F). The parental tissue showed accumulation of HER2 expression in distinct tumor cell clusters, whereas the PDX sample showed a more diffused expression of HER2 on the epithelial cells (Figure 4G).

Taken together, we have shown the establishment of a subcutaneous GC-PDX model, which resembled human GC histology and maintained the tumor mutations.

Orthotopic GC-PDX Model

Subcutaneous grafts are valuable and provide easy access to monitor tumor growth by caliper, but do not take the original, local tumor environment into account. To mimic this, we developed an orthotopic GC graft model (oPDX). 1–2 mm Pieces of the previously established subcutaneous GC-PDX tumors were engrafted onto the gastro-esophageal junction in NSG recipient mice (Figure 5A and B). All mice (n=5) were successfully transplanted and showed subsequent tumor growth.

Tumors were allowed to grow for 66 days before mice were sacrificed. Weights of the mice were stable until day 50 when mice started to lose some weight (Supplementary Figure 4). To showcase feasibility of tumor volume monitoring in vivo, a small set of PDX tumors (n=3) were orthotopically engrafted as described above. Three weeks after engraftment, tumors were monitored by non-invasive ultrasound imaging, displaying volumes from 18.81 to 67.9 mm^3 (Figure 5C). High blood flow to the tumor area was observed by the presence of vessels, suggesting engagement of the engrafted tumor in the stomach. At sacrifice, large tumors were found growing into the abdominal space and into the stomach lumen (Figure 5D).

Upon processing and analysis of pan-CK and vimentin, stroma-rich tumors were observed, which resembled the parental tissues. αSMA and Alcian blue stainings showed slightly less activated fibroblasts and varying amounts of mucus-producing cells between the two analyzed tumors when compared to parental tissue (Figures 4E and 5E). These tumors were highly proliferative, had low apoptotic rates and showed vasculature similar to the parental tissue, depicted by the Ki67, CC3 and endoglin stainings (Figures 4F and 5F). PDX samples showed dim HER2 staining on the epithelial cells (Figures 4G and 5G).

Taken together, these data show that we robustly established an orthotopic GC model, resulting in stroma-rich tumors at the original site of tumor development.

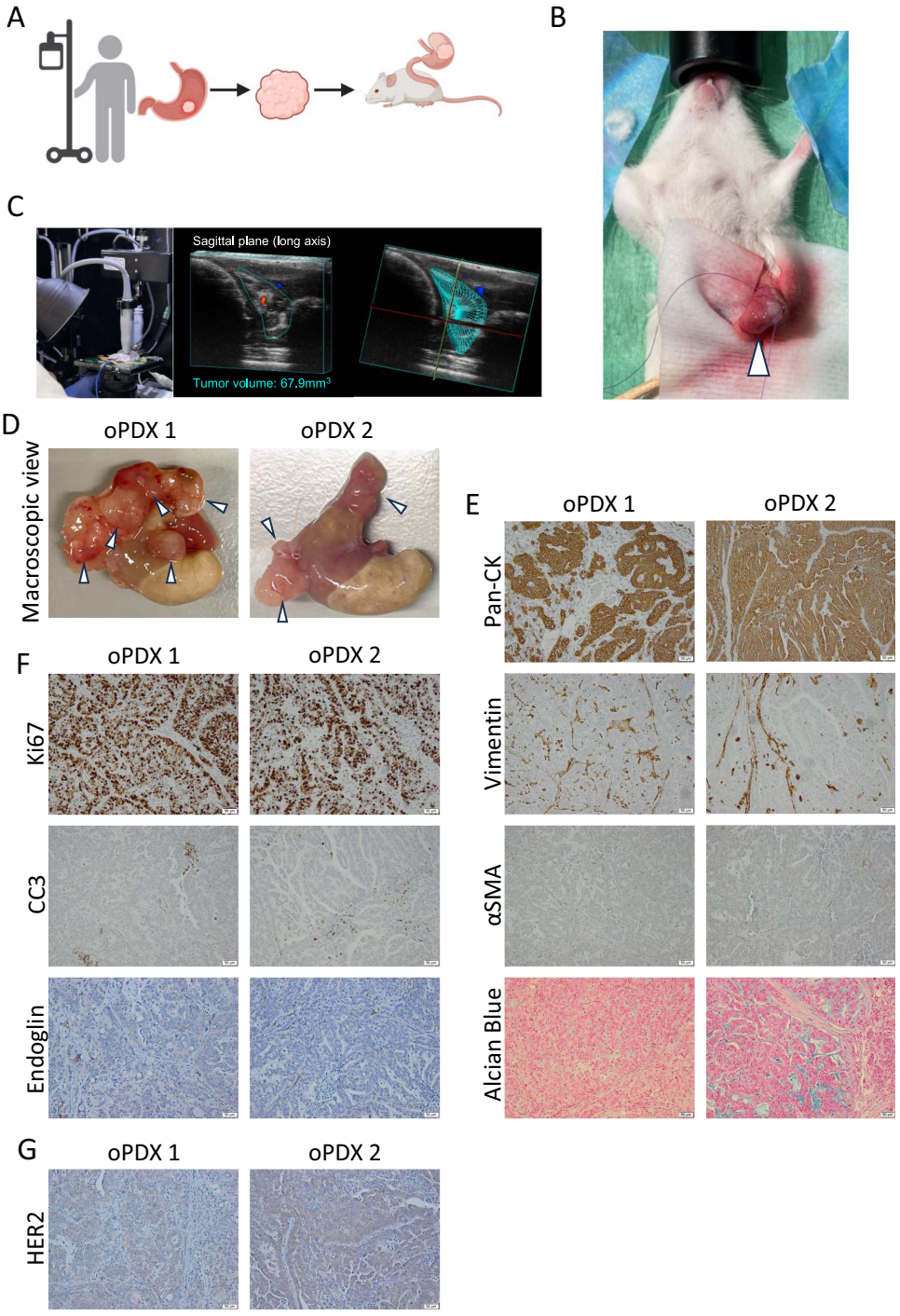

Figure 5 Establishment and evaluation of an orthotopic gastric cancer model. (**A** and **B**) human gastric cancer tissue was orthotopically engrafted into the stomach of NSG mice (arrowpoint). (**C**) Ultrasound images of the tumors at week 3 post engraftment. Images were obtained in the sagittal plane (long axis) with the MX550D transducer at an axial resolution of 40 µm and analyzed using the Vevo LAB 5.8.2 software. (**D**) Macroscopic images of stomach with the engrafted gastric tumor after sacrifice. Arrows indicate tumor tissue. (**E**), (**F** and **G**) Tumors were evaluated for presence of epithelial, stromal, and tumor markers via immunohistochemistry. Scale bar represents 50 µm. *Created in BioRender. Zonneveld, J (2026)* https://BioRender.com/hid80uq.

Abbreviations: Pan-CK, pan-cytokeratin; αSMA, alpha-smooth muscle actin; CC3, cleaved-caspase 3; HER2, human epidermal growth factor receptor 2.

Discussion

In this study, we show establishment of advanced preclinical in vitro and in vivo fibroblast-rich models for GC, which are representative for the parental tissues they were derived from. The establishment of multicellular models for GC opens

up new possibilities to assess drug efficacy in a preclinical setting which more closely resembles GC tumors and the local TME.

Drug development in oncology is a relatively inefficient process with high costs and high failure rates, which is shown by the fact that 85–89% of anticancer drugs that enter the preclinical testing phase do not obtain regulatory approval, due to not enough efficacy in patients.[25] These alarming failure rates showcase the high need for more accurate preclinical disease models.

Preclinical phases of drug development usually start with a wide range of in vitro cell based models. However, the majority of the cancer cell lines that are currently used are originally derived from patients many years ago and have been cultured as single 2D immortalized cells. These cells are typically more susceptible to clonal adaptation and selection, with significant phenotypic and genetic shifts from the original patient's tumor. The development of preclinical in vitro cancer models has seen a rapid rise in the past decades with the development of organoid technology. Tumor-specific characteristics, strong replication potential and the presence of multiple epithelial cell types in a 3D environment make organoids a superior model compared to regular monolayer culture of long grown cell lines.[26] The present study shows that patient-derived features can be successfully maintained in vitro in the established GC-PDOs, based on histology and mutation analysis. Considering a panel of patient-derived models displaying different mutational spectra, patients could potentially be further stratified and drugs optimally tested.

However, although valuable, in vitro models lack crucial components of the tumor microenvironment, especially the tumor stroma. We showed that generation of a GC mini-tumor model consisting of PDOs and CAFs is feasible and reproducible. These mini-tumors resemble the parental tissue, the cellular components they were derived from and are a valuable tool for drug testing and patient stratification. GC mini-tumors were cultured up to 7 days, and can be exposed to various drugs and treatments, and allow to further investigate the spatial distribution and the response/interaction of the included cells of interest. Recent studies have also highlighted the value of ex vivo tumor explants, where whole tumor pieces are cultured over a short period of time. While tumor explants are able to maintain the original tumor architecture, they are also more heterogeneous and tissue-dependent, since every section has a different cell content, making it more difficult to be a reproducible and scalable platform. Explants are hard to culture over time, due to the complex media, materials and instruments needed to maintain O_2 levels. Compared to tumor explants, mini-tumors enable investigation into mechanisms-of-action and cell interaction in a more controlled manner. Due to the scarceness of patient material, isolation of PDOs and fibroblasts might be preferable in order to expand the material and generate multiple mini-tumors to allow for more extensive drug testing.[27]

While in vitro testing remains to be highly valuable and cost effective, not all aspects of the tumor environment, physiological processes and other cell compartments, are captured in this setting. To tackle this, we developed various in vivo models, which better represent the GC tumor environment, development and progression. We showed that after in vitro expansion, GC-PDOs can be successfully injected subcutaneously into mice, resulting in stroma-rich tumors. The same goes for the subcutaneously engrafted GC tumor pieces. Both models resulted in tumors that resembled the parental tissues, based on histology and mutational data. However, an APC mutation was detected in the PDX tissue, which was not present in its parental sample. This mutation might have been enriched in the PDX or alternatively has been below the detection limit in the primary tumor. These engrafting methods also allow for expansion of rare patient material which can be serially reimplanted in new mice. We show that PDX tissue can also be stored frozen before reimplantation or in vitro experiments, indicating the possibility for the generation of a biobank.

In order to better resemble the original site of GC development, we orthotopically transplanted GC pieces onto the stomach of mice. Although this is a more invasive and challenging method, and tumors are more difficult to measure by caliper, monitoring is possible via ultrasound imaging. This imaging technique can be used for multiple purposes such as estimating tumor location, quantifying tumor volume upon certain treatment, measuring angiogenic tumor capacity, and tracking labelled agents. Two months after engraftment, large stroma-rich tumors were found to grow into the abdominal space and into the stomach lumen. These tumors also resembled the parental tumors on a histological level, showcasing their ability to maintain their phenotype in a different environment. Although orthotopic tumors require specialized equipment such as ultrasound to measure tumors, this model might be favored when studying tumor metastasis. The transplantation site is also known to influence key processes such as tumor engraftment, proliferation, and metastasis and should be chosen carefully taking into account the research question.[28]

Table 2 Summary of Important Characteristics Associated with Each GC Model Using a Scoring System

Model	Difficulty	Resemblance	System	Duration	Throughput
PDOs	■□□□	Single cell type	In vitro	■□□□	■■■□
Mini-tumor model	■■□□	Multiple cell types, Fully human stroma	In vitro	■□□□	■■■□
Subcutaneous ODX model	■■□□	Multiple cell types, Mouse stroma	In vivo	■□□□	■■□□
Subcutaneous PDX model	■■□□	Multiple cell types, Mouse stroma	In vivo	■■■□	■□□□
Orthotopic PDX model	■■■□	Original site, Multiple cell types, Mouse stroma	In vivo	■■□□	■□□□

Notes: (□□□□ = lowest score, ■■■■ = highest score).

Previously, we have described multicellular, fibroblast-rich models for pancreatic and colorectal cancer.[20,22] These models showed high histological similarities to parental tumor tissues and differentiation into various CAF subsets. In this study, we describe similar models for GC, where patient characteristics are strongly maintained (Table 2). These models should eventually be evaluated in their ability to resemble and predict the patient's therapy responses, which could contribute greatly to personalized treatment decisions and preclinical testing of novel therapeutics.

Conclusion

We have established five close-to-patient models for GC which might aid in developing better therapies for GC. Histological and genetic evaluation show some useful similarities between patient material and the established models. These models can be exploited in the future to predict therapy responses or to test the efficacy and safety of new treatment strategies in a more high throughput manner by performing drug screens.

Funding

This work was supported by research grants from the Dutch Cancer Society (KWF) project 14974 and project 15829 and Flanders Institute for Research and InnovationHBC.2018.2002 and HBC.2021.0759. The collaboration project is co-funded by PPP allowance made available by Health~Holland, Top Sector Life Sciences & Health, to stimulate public-private partnerships.

Disclosure

LH and MS are members of the scientific advisory board of InnoSer laboratories (without financial compensation), developing close-to-patient models for cancer research. LH has received consultancy fees from InnoSer laboratories related to the development of IBD models (not related to this work). SH was an employee of InnoSer laboratories during the time part of these studies were performed and reports grants from VLAIO. InnoSer had no influence in the design, performance or analysis of the data presented in this manuscript. AVW reports personal fees from Johnson & Johnson Innovative Medicine, Biologics, outside the submitted work. The authors report no other conflicts of interest in this work.

References

1. Bray F, Laversanne M, Sung H, et al. Global cancer statistics 2022: GLOBOCAN estimates of incidence and mortality worldwide for 36 cancers in 185 countries. *CA Cancer J Clin*. 2024;74(3):229–263. doi:10.3322/caac.21834
2. Mamun TI, Younus S, Rahman MH. Gastric cancer—Epidemiology, modifiable and non-modifiable risk factors, challenges and opportunities: an updated review. *Cancer Treat Res Commun*. 2024/01;41. doi:10.1016/j.ctarc.2024.100845.
3. Lordick F, Carneiro F, Cascinu S, et al. Gastric cancer: ESMO clinical practice guideline for diagnosis, treatment and follow-up. *Ann Oncol*. 2022;33 (10):1005–1020. doi:10.1016/j.annonc.2022.07.004
4. Smyth EC, Nilsson M, Grabsch HI, van Grieken NC, Lordick F. Gastric cancer. *Lancet*. 2020;396(10251):635–648. doi:10.1016/s0140-6736(20) 31288-5
5. Li K, Zhang A, Li X, Zhang H, Zhao L. Advances in clinical immunotherapy for gastric cancer. *Biochim Biophys Acta Rev Cancer*. 2021;1876 (2):188615. doi:10.1016/j.bbcan.2021.188615

6. Liu J, Yuan Q, Guo H, Guan H, Hong Z, Shang D. Deciphering drug resistance in gastric cancer: potential mechanisms and future perspectives. *Biomed. Pharmacother.* 2024;173:11631. doi:10.1016/j.biopha.2024.116310
7. Kemi N, Eskuri M, Herva A, et al. Tumour-stroma ratio and prognosis in gastric adenocarcinoma. *Br. J. Cancer.* 2018;119(4):435–439. doi:10.1038/s41416-018-0202-y
8. Valkenburg KC, Pienta KJ, de Groot AE, et al. Targeting the tumour stroma to improve cancer therapy. *Nat Rev Clin Oncol*. 2018;15(6):366–381. doi:10.1038/s41571-018-0007-1
9. Oya Y, Hayakawa Y, Koike K. Tumor microenvironment in gastric cancers. *Cancer Sci*. 2020;111(8):2696–2707. doi:10.1111/cas.14521
10. Abudukelimu S, de Miranda NFCC, Hawinkels LJAC. Fibroblasts in orchestrating colorectal tumorigenesis and progression. *CMGH*. 2024;17(5):821–826. doi:10.1016/j.jcmgh.2024.01.013
11. Yasuda K, Torigoe T, Mariya T, et al. Fibroblasts induce expression of FGF4 in ovarian cancer stem-like cells/cancer-initiating cells and upregulate their tumor initiation capacity. *Lab Invest*. 2014;94(12):1355–1369. doi:10.1038/labinvest.2014.122
12. Zhao X-L, Lin Y, Jiang J, et al. High-mobility group box 1 released by autophagic cancer-associated fibroblasts maintains the stemness of luminal breast cancer cells - PubMed. *J Pathol*. 2017;243(3):376–389. doi:10.1002/path.4958
13. Wegner C, Hauge A, Gaustad J, et al. Dynamic contrast-enhanced MRI of the microenvironment of pancreatic adenocarcinoma xenografts - PubMed. *Acta oncologica*. 2017;56(12):1754–1762. doi:10.1080/0284186X.2017.1343494
14. Provenzano P, Cuevas C, Chang A, Goel V, Hoff DV, Hingorani S. Enzymatic targeting of the stroma ablates physical barriers to treatment of pancreatic ductal adenocarcinoma - PubMed. *Cancer Cell*. 2012;21(3):418–429. doi:10.1016/j.ccr.2012.01.007
15. Ozerdem U, Hargens AR. A simple method for measuring interstitial fluid pressure in cancer tissues. *Microvascular Res*. 2005;70(1–2):116–120. doi:10.1016/j.mvr.2005.07.003
16. Munson J, Bellamkonda R, Swartz M. Interstitial flow in a 3D microenvironment increases glioma invasion by a CXCR4-dependent mechanism - PubMed. *Cancer Res*. 2013;73(5):1536–1546. doi:10.1158/0008-5472.CAN-12-2838
17. Hirth J, Watkins PB, Strawderman M, Schott A, Bruno R, Baker LH. The effect of an individual's cytochrome CYP3A4 activity on docetaxel clearance. *Clin Cancer Res*. 2000;6(4):1255–1258.
18. Hakuno SK, Michiels E, Kuhlemaijer EB, Rooman I, Hawinkels L, Slingerland M. Multicellular modelling of difficult-to-treat gastrointestinal cancers: current possibilities and challenges. *Int J Mol Sci*. 2022;23(6). doi:10.3390/ijms23063147
19. Bidan N, Dunsmore G, Ugrinic M, et al. Multicellular tumor spheroid model to study the multifaceted role of tumor-associated macrophages in PDAC. *Drug Deliv Transl Res*. 2024;14(8):2085–2099. doi:10.1007/s13346-023-01479-5
20. Harryvan TJ, Hawinkels L, Östman A, Ten Dijke P, Strell C, Hornsveld M. A novel pancreatic cancer mini-tumor model to study desmoplasia and myofibroblastic cancer-associated fibroblast differentiation. *Gastro Hep Adv*. 2022;1(4):678–681. doi:10.1016/j.gastha.2022.04.019
21. Bartfeld S, Bayram T, Mvd W, et al. In vitro expansion of human gastric epithelial stem cells and their responses to bacterial infection. *Gastroenterology*. 2015;148(1):126–136.e6. doi:10.1053/j.gastro.2014.09.042
22. Dang H, Harryvan TJ, Liao CY, et al. Cancer-associated fibroblasts are key determinants of cancer cell invasion in the earliest stage of colorectal cancer. *Cell Mol Gastroenterol Hepatol*. 2023;16(1):107–131. doi:10.1016/j.jcmgh.2023.04.004
23. Schoonderwoerd MJA, Hakuno SK, Sassen M, et al. Targeting endoglin expressing cells in the tumor microenvironment does not inhibit tumor growth in a pancreatic cancer mouse model. *Onco Targets Ther*. 2021;14:5205–5220. doi:10.2147/OTT.S322276
24. Cohen D, Hondelink LM, Solleveld-Westerink N, et al. Optimizing mutation and fusion detection in nsclc by sequential dna and rna sequencing. *J Thorac Oncol*. 2020;15(6):1000–1014. doi:10.1016/j.jtho.2020.01.019
25. Koga Y, Ochiai A, Ochiai A, Koga Y, Ochiai A. Systematic review of patient-derived xenograft models for preclinical studies of anti-cancer drugs in solid tumors. *Cells*. 2019;8:418. doi:10.3390/cells8050418
26. Drost J, Clevers H. Organoids in cancer research. *Nat Rev Cancer*. 2018;18(7):407–418. doi:10.1038/s41568-018-0007-6
27. Wu KZ, Adine C, Mitriashkin A, BJJ A, Iyer NG, Fong ELS. Making in vitro tumor models whole again. *Adv. Healthcare Mater*. 2023;12(14). doi:10.1002/adhm.202202279
28. Kang W, Maher L, Michaud M, et al. Development of a novel orthotopic gastric cancer mouse model. *Biological Procedures Online*. 2021;23(1). doi:10.1186/s12575-020-00137-1